Materials Science-Poland, *Vol. 28*, *No. 1*, *2010*

Electrical conduction in $Ba(Bi_{0.5}Nb_{0.5})O_3$ ceramics Impedance spectroscopy analysis

K. PRASAD[1*], S. BHAGAT[1], K. AMARNATH[1], S.N. CHOUDHARY[1], K.L. YADAV[2]

[1] Materials Research Laboratory, University Department of Physics, T.M. Bhagalpur University, Bhagalpur 812 007, India

[2] Department of Physics, Indian Institute of Technology, Roorkee 247 667, India

A new lead free perovskite ceramics $Ba(Bi_{0.5}Nb_{0.5})O_3$ was fabricated by a conventional ceramic technique at 1185 °C and subsequent sintering at 1200 °C in air atmosphere. The XRD analysis of $Ba(Bi_{0.5}Nb_{0.5})O_3$ powder indicated the formation of a single-phase monoclinic structure. The ac conductivity data were found to obey the power law and showed a negative temperature coefficient for the resistance behaviour. The ac conductivity values were used to evaluate the density of states at the Fermi level, minimum hopping length and activation energy of the compound. The correlated barrier hopping model was found to successfully explain the mechanism of charge transport in $Ba(Bi_{0.5}Nb_{0.5})O_3$.

Keywords: *$Ba(Bi_{0.5}Nb_{0.5})O_3$; ceramics; ac conductivity; conduction mechanism; hopping model*

1. Introduction

$A(B'B'')O_3$ materials of the perovskite type exhibiting high dielectric permittivity ε' are of current interest due to their practical applications in various electronic/microelectronic devices. Most of the materials used for these applications are, in general, lead bearing compounds, e.g. $PbTiO_3$, $PbZr_{1-x}Ti_xO_3$, $PbMg_{1/3}Nb_{2/3}O_3$, $PbFe_{1/2}Nb_{1/2}O_3$, etc. With the aim of identifying alternatives to the lead-based materials, the electrical properties of $Ba(Fe_{1/2}Nb_{1/2})O_3$ [1–9], $Ba(Al_{1/2}Nb_{1/2})O_3$ [10], $Sr(Fe_{1/2}Nb_{1/2})O_3$ [5], $Ba(Fe_{1/2}Ta_{1/2})O_3$ [11], etc. have been investigated. One such ceramics in this series is perovskite $Ba(Bi_{0.5}Nb_{0.5})O_3$ having the tolerance factor $t = 0.8769$ estimated using the relation:

$$t = \frac{r_{Ba} + r_O}{\sqrt{2}}\left(\frac{r_{Bi} + r_{Nb}}{2} + r_0\right)^{-1}$$

*Corresponding author, e-mail: k.prasad65@gmail.com

where r_{Ba}, r_{Bi}, r_{Nb} and r_O are the ionic radii of the constituent ions. The material is mechanically tough and lead-free.

The complex impedance spectroscopy technique is widely recognized as a non-destructive but powerful technique for the study of the electrical properties of solids [12]. Thus, the dynamics of ionic movement and the contributions of various microstructure elements such as grain, grain boundary and interfacial polarization, to total electric response in polycrystalline solids can be identified by this technique. It also enables us to evaluate the nature of dielectric relaxation and the relaxation frequency of the material.

Despite an extensive literature survey, there has been no study of $Ba(Bi_{0.5}Nb_{0.5})O_3$ (BBN) so far, to the best of the author's knowledge. In the present work, structural, microstructural and ac conductivity studies of BBN have been described. An attempt has also been made to explain the conduction mechanism in the system.

2. Experimental

$Ba(Bi_{0.5}Nb_{0.5})O_3$ (BBN) was obtained from AR grade (99.9%+ pure) chemicals ($BaCO_3$, Bi_2O_3 and Nb_2O_5) by solid state synthesis using the following chemical reaction at 1185 °C for 4 h:

$$BaCO_3 + \frac{1}{4}Bi_2O_3 + \frac{1}{4}Nb_2O_5 \xrightarrow{\Delta} Ba(Bi_{0.5}Nb_{0.5})O_3 + CO_2$$

under controlled heating and cooling cycles. A circular disc shaped pellet, 9.99 mm in diameter and 2.192 mm thick was made by applying a uniaxial stress of ca. 650 MPa. The pellet was subsequently heated up to 1200 °C under air for 3h. The complete reaction and the formation of the desired compound were verified by X-ray diffraction analysis. The weights of the samples were monitored before and after heat treatments. The maximum difference was about 1.08 mg for 10 g of the sample. Therefore, the compositions of the samples were considered to be the same as the initial ones. The XRD spectra were taken on calcined powder of BBN with a X-ray diffractometer (XPERT-PRO) at room temperature, using CuK_α radiation (λ = 1.5405 Å), over a wide range of Bragg angles ($20° \le 2\theta \le 80°$) with a scanning speed of $2°\cdot min^{-1}$. The microstructure of the sintered BBN sample was taken on the fractured surface using a computer controlled scanning electron microscope (SEM Hitachi S-3400N, Japan). The identification of secondary phases present in the sample was carried out using an energy dispersive X-ray analyzer (Thermo Noran NSS200). Electrical impedance Z, phase angle θ, loss tangent $\tan\delta$ and capacitance C were measured in function of frequency (0.1 kHz–1 MHz) at various temperatures (30–500 °C) using a computer controlled LCR Hi-Tester (HIOKI 3532-50), Japan, attached with a microprocessor controlled dry temperature controller (DPI-1100), Sartech Intl., India on a symmetrical cell of type Ag|ceramics|Ag, where Ag is a conductive paint coated on either side of the pellet.

3. Results and discussion

Figure 1 shows the XRD profile of calcined BBN powder. A standard computer program (POWD) was utilized for the XRD profile analysis. Good agreement between the observed and calculated inter-planar spacing and no traces of any extra peaks due to constituent oxides were found, thereby suggesting the formation of a single phase compound having a monoclinic structure. The lattice parameters were estimated to be a = 4.320(6) Å, b = 4.238(8) Å, c = 3.001(6) Å and β = 90.659° with the estimated error of $\pm 10^{-4}$ Å. The unit cell volume was estimated to be 54.97 Å^3.

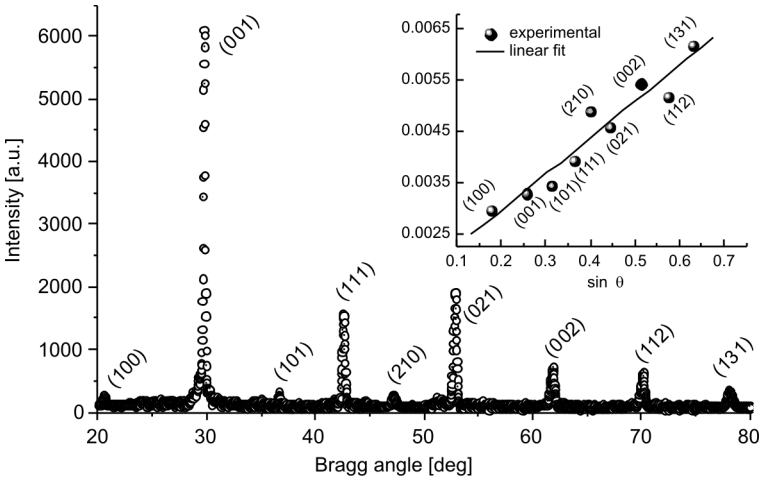

Fig. 1. X-ray diffraction pattern of calcined $Ba(Bi_{0.5}Nb_{0.5})O_3$ powder at room temperature. Inset shows the Williamson–Hall plot

The XRD pattern of BBN is found to be similar to that of $Ba(Fe_{0.5}Nb_{0.5})O_3$ [3, 6, 7, 9] with little shifts in peak positions. This may be due to the difference in the ionic radii of Fe^{3+} and Bi^{3+} ions. The criterion adopted for evaluating the robustness and accuracy of of the indexing and the structure of compound was the sum of differences in observed and calculated d values (i.e., $\sum \Delta d = \sum (d_{obs} - d_{calc})$), which were minimized using a least squares refinement technique. The apparent particle size and lattice strain of BBN were estimated by analyzing the broadening of the X-ray diffraction peak, using the Williamson–Hall approach [13]:

$$\beta \cos\theta = \frac{K\lambda}{D} + 2\frac{\Delta\xi}{\xi}\sin\theta \tag{1}$$

where D is the apparent particle size, β is the width of the diffraction peak at half intensity (FWHM), $\Delta\xi/\xi$ is the lattice strain and K is the Scherrer constant (K = 0.89). The term $K\lambda/D$ represents the Scherrer particle size distribution. The Gaussian model was applied to estimate the width of the diffraction peak at half intensity.

$$I = I_0 + \frac{A}{\eta\sqrt{\frac{\pi}{2}}}\exp\left(-2\left(\frac{\theta-\theta_c}{\eta}\right)^2\right) \tag{2}$$

where A and θ_c are the area and centre of the curve, respectively. The inset of Fig. 1 illustrates the Williamson–Hall plot for BBN. A linear least squares fitting of the $\beta\cos\theta$–$\sin\theta$ data provided the values of the apparent particle size and the lattice strain: these were found to be approximately 89 nm and 0.0035, respectively.

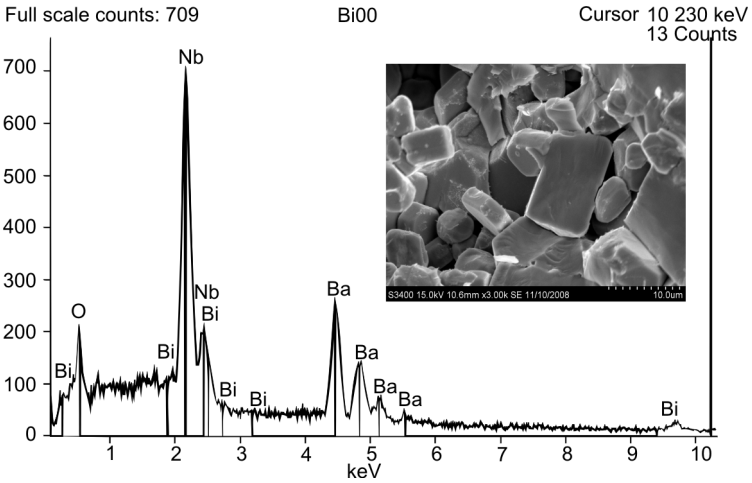

Fig. 2. EDAX spectrum and SEM micrograph of fractured surface of $Ba(Bi_{0.5}Nb_{0.5})O_3$ ceramics

To confirm the absence of a second phase, EDAX was carried out. Figure 2 shows the EDAX pattern for the constituent ions of BBN. All peaks in the pattern match perfectly with the elements present in $Ba(Bi_{0.5}Nb_{0.5})O_3$. This clearly indicated the purity and formation of BBN. The grain shapes (almost cuboid) are clearly visible in the SEM micrograph (inset of Fig. 2) of the sintered BBN sample, indicating the existence of a polycrystalline microstructure. Grains of unequal sizes (5–10 μm) appear to be distributed throughout the sample.

The ac electrical conductivity, which in most of the materials is due to localized states, is given by:

$$\sigma_{ac} = \sigma(0) + \sigma(\omega) \tag{3}$$

where $\sigma(0)$ and $\sigma(\omega)$ are the frequency independent and frequency dependent parts of the conductivity, respectively. Also, $\sigma(\omega)$ was found to satisfy the following equation in the frequency sensitive region: $\sigma(\omega) = A\omega^s$ with $0 \leq s \leq 1$, ω being the angular frequency of the applied ac field and $A = \pi N^2 e^2/6k_BT(2\alpha)$ is a constant, e is the electron charge, T – temperature, α – polarizability of a pair of sites, and N – the number of sites per unit volume among which hopping takes place. Such variation is associated

with displacement of carriers which move within the sample by discrete hops of the length R between randomly distributed localized sites. The term $A\omega^s$ can often be described based on two distinct mechanisms for carrier conduction: (i) quantum mechanical tunnelling (QMT) through the barrier separating the localized sites; and (ii) correlated barrier hopping (CBH) over the same barrier. In these models, the exponent s is found to have two different trends being a function of temperature and frequency. If the ac conductivity is related to QMT, s is predicted to be temperature independent but is expected to show a decreasing trend with ω

$$s = 1 + \frac{4}{\lg(\omega\tau_0)} \tag{4}$$

where τ_0 is the characteristic relaxation time. The ac conductivity is expected to be [14]

$$\sigma_{ac} = \frac{\pi^4}{24} e^2 \omega k_B T \left(N\left(E_f\right)\right)^2 \alpha^{-1} R_\omega^4 \tag{5}$$

where α^{-1} is the spatial decay parameter for the localized wave function, and R_ω is the tunnelling length at the frequency ω. If ac conductivity is related to CBH [15],

$$\sigma_{ac} = \frac{\pi}{3} e^2 \omega k_B T \left(N\left(E_f\right)\right)^2 \alpha^{-5} \left(\ln\frac{f_0}{\omega}\right)^4 \tag{6}$$

where $N(E_f)$ is the density of states at the Fermi level, f_0 the photon frequency and α is the localized wave function. The exponent s and minimum hopping length $R_{\min}$ can be expressed as [16, 17]

$$s = 1 - \frac{6k_B T}{W_m} \tag{7}$$

$$R_{\min} = \frac{2e^2}{\pi\varepsilon\varepsilon_0 W_m} \tag{8}$$

where W_m is the binding energy, which is defined as the energy required to remove an electron completely from one site to the another site. Figure 3 shows the log–log dependence of the electrical conductivity on frequency at various temperatures. The pattern of the conductivity spectrum shows dispersion throughout the chosen frequency range. The frequency dependence of ac conductivity satisfies [18]:

$$\sigma_{ac} = A_1\omega^{S_1} + A_2\omega^{S_2} \tag{9}$$

where A_1 and A_2 are the temperature dependent constants, and s_1 and s_2 are temperature as well as frequency dependent parameters. The values of s_1 and s_2 can be obtained from the slopes of the plots: $\lg\sigma_{ac}$ vs. $\lg\omega$ in the low and high frequency regions. The inset of Fig. 3 shows the temperature dependence of s_1 and s_2. It can be seen that the values of both s_1 and s_2 are always lower than 1. Also, the values of both s_1 as well as s_2 decrease with the rise in temperature. The value of $s_1 \to 0$ at higher

temperatures indicates that the dc conductivity dominates at higher temperatures in the low frequency region satisfying Eq. (3). The model based on correlated hopping of electrons over a barrier [19] predicts a decrease in the value of s_1 with the increase in temperature, and thus it is found to be consistent with the experimental results. Therefore, the conduction in the system could be considered due to the short range translational type hopping of charge carriers [18–20]. This indicates that the conduction process is thermally activated.

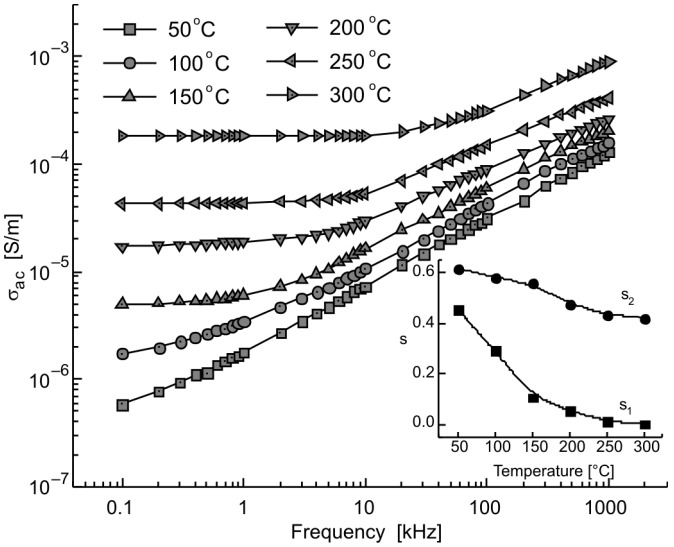

Fig. 3. Dependences of ac conductivity on frequency at various temperatures for $Ba(Bi_{0.5}Nb_{0.5})O_3$ ceramics. Inset figure illustrates the dependences of s_1 and s_2 on temperature

The hopping conduction mechanism is generally consistent with the existence of high density of states in the materials having a band gap similar to that of a semiconductor. Due to localization of charge carriers, formation of polarons takes place and the hopping conduction may occur between the nearest neighbouring sites. Figure 4 shows the dependence of ac conductivity on $10^3/T$. The activation energy for conduction was determined using the Arrhenius relationship:

$$\sigma_{ac} = \sigma_0 \exp\left(-\frac{E_a}{k_B T}\right) \tag{10}$$

where E_a is the activation energy of conduction and T is the absolute temperature. The variation profile shows the negative temperature coefficient of resistance (NTCR) behaviour of BNN. A linear least squares fitting of the conductivity data to Eq. (10) gives the value of the activation energy, E_a. The values of E_a were found to be 0.379 eV, 0.352 eV and 0.349 eV at 1 kHz, 10 kHz and 100 kHz, respectively.

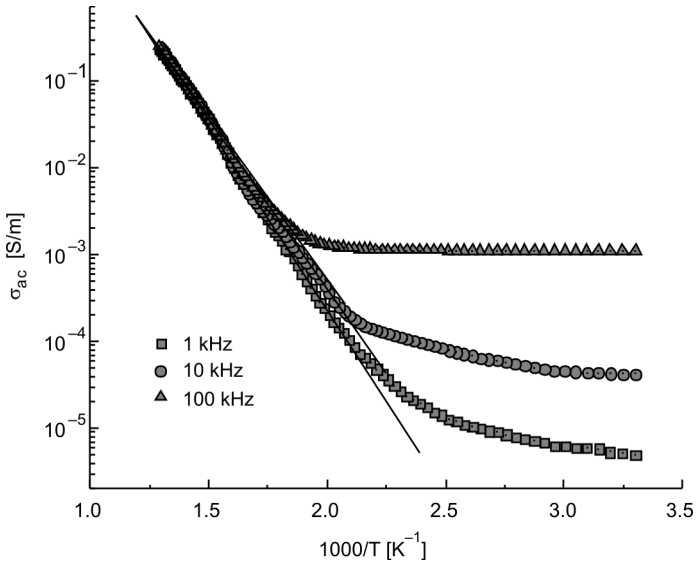

Fig. 4. Dependences of ac conductivity on inverse of temperature at various frequencies for $Ba(Bi_{0.5}Nb_{0.5})O_3$ ceramics

The activation energy decreases with the increase in frequency It can be seen that the ac conductivity is almost frequency insensitive in low temperature region. Also, the onset temperature shifts to higher temperature side with the increment in frequency. The low value of E_a may be due to the carrier transport through hopping between localized states in a disordered manner [21]. The increase in conductivity with temperature may be explained, taking into consideration that within the bulk the oxygen vacancies due to the loss of oxygen, are usually created during sintering and the charge compensation is described by the following reaction [22]:

$$O \rightarrow \tfrac{1}{2}O_2 \uparrow + V_0^{\bullet\bullet} + 2e^-$$

which may leave behind free electrons, making them n type [23].

The values of $N(E_f)$ were estimated using Eq. (6) by assuming $f_0 = 10^{13}$ Hz, $\alpha = 10^{10}$ m^{-1} at various operating frequencies and temperatures. Figure 5 shows the frequency dependence of $N(E_f)$ at various temperatures. It can be seen that the values of $N(E_f)$ decrease with the increase in the operating frequency. Inset of Fig. 5 shows the variation of $N(E_f)$ with temperature at various frequencies. It is seen that the $N(E_f)$ simply increases with the increase in temperature. Therefore, at low frequencies the electrical conduction in the system is being affected by both frequency as well as temperature, whereas at higher frequencies the charge carriers are localized and being affected by thermal excitations. The reasonably high values of $N(E_f)$ suggest that the hopping between the pairs of sites dominates the mechanism of charge transport in BBN.

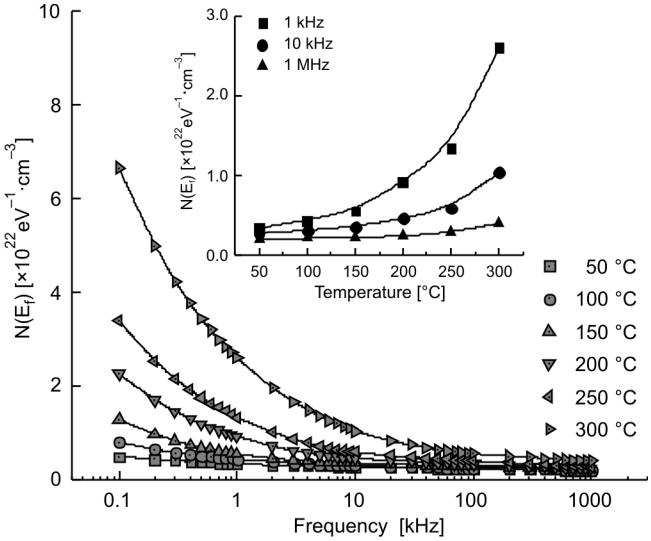

Fig. 5. Dependences of density of states at Fermi level of $(Ba(Bi_{0.5}Nb_{0.5})O_3$ ceramics on frequency at various temperatures. Inset figure shows the temperature dependence of $N(E_f)$ at various frequencies

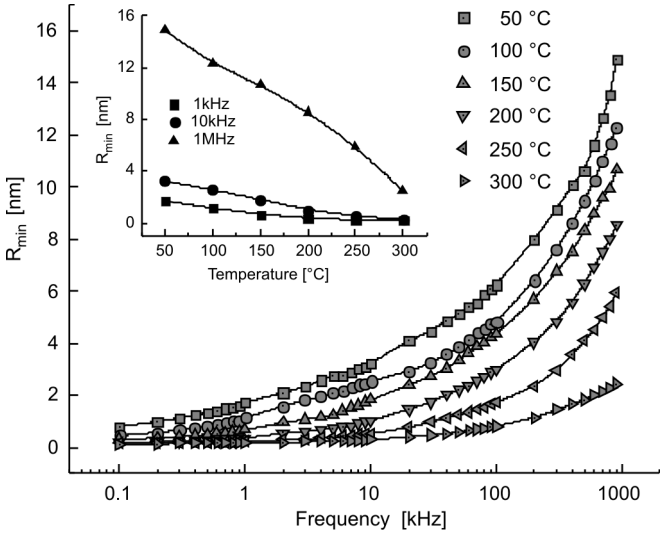

Fig. 6. Dependences of R_{min} of $Ba(Bi_{0.5}Nb_{0.5})O_3$ ceramics on frequency at various temperatures. Inset figure shows the variation of R_{min} on temperature at various frequencies

The values of the minimum hopping distance, R_{min} were calculated using Eq. (8). Figure 6 presents the variation of R_{min} with frequency at various temperatures. The values of R_{min} simply increase as the frequency increases at every temperature. Inset of Fig. 6 shows the variation of R_{min} with temperature at various frequencies. It can be seen that the values of R_{min} decrease with the increase in temperature. The value of R_{min} at room temperature was found to be 1.6 nm.

4. Conclusions

Polycrystalline $Ba(Bi_{0.5}Nb_{0.5})O_3$, fabricated through a high-temperature solid state reaction technique, was found to have a single phase perovskite type monoclinic structure. The ac conductivity is found to obey the universal power law and showed the NTCR character. The correlated barrier hopping model is found to successfully explain the mechanism of charge transport in BBN. Furthermore, the frequency dependent ac conductivity at various temperatures indicated that the conduction process is thermally activated.

Acknowledgements

The present work was supported by the Defense Research and Development Organization, New Delhi.

References

[1] REANEY I.M., PETZELT J., VOITSEKHOVSKII V.V., CHU F., SETTER N., J. Appl. Phys., 76 (1994), 2086.
[2] SAHA S., SINHA T.P., Phys. Rev. B, 65 (2002), 134103.
[3] RAEVSKI I.P., PROSANDEEV S.A., BOGATIN A.S., MALITSKYA M.A., JASTRABIK L., J. Appl. Phys., 93 (2003), 4130.
[4] CHUNG C.-Y., CHANG Y.-H., CHEN G.-J., J. Appl. Phys., 96 (2004), 6624.
[5] CHUNG C.-Y., CHANG Y.-H., CHEN G.-J., CHAI Y.-L., J. Cryst. Growth, 284 (2005), 100.
[6] EITSSAYEAM S., INTATHA U., PENGPAT K., TUNKASIRI T., Curr. Appl. Phys., 6 (2006), 316.
[7] WANG Z., CHEN X.M., NI L., LIU X.Q., Appl. Phys. Lett., 90 (2007), 022904.
[8] INTATHA U., EITSSAYEAM S., PENGPAT K., MACKENZIE K.J.D., TUNKASIRI T., Mater. Lett., 61 (2007), 196.
[9] KE S., HUANG H., FAN H., CHAN H.L.W., ZHOU L.M., Ceram. Int., 34 (2008), 1059.
[10] DUTTA A., SINHA T.P., J. Phys. Chem. Solids, 67 (2006), 1484.
[11] JUNG W.-H., LEE J.-H., SOHN J.-H., NAM H.-D., CHO S.-H., Mater. Lett., 56 (2002), 334.
[12] SUMAN C.K., PRASAD K., CHOUDHARY R.N.P., Adv. Appl. Ceram., 104 (2005), 294.
[13] WILLIAMSON G.K., HALL W.H., Acta. Metall., 1 (1953), 22.
[14] ELLIOTT S.R., Adv. in Phys., 36 (1987), 135.
[15] SHARMA G., ROY M., ROY M.S., Mater. Sci. Eng., B 104 (2003), 15.
[16] MOLLAH S., SOM K.K., BOSE K., CHAUDRI B.K., J. Appl. Phys., 74 (1993), 931.
[17] SALAM R., Phys. Stat. Sol. (a), 117 (1990), 535.
[18] FUNKE K., Prog. Solid State Chem., 22 (1993), 111.
[19] ELLIOTT S.R., Philos. Mag., B 37 (1978), 553.
[20] YOUSSEF AHMED A.A., Z. Naturforsch., A57 (2002), 263.
[21] PRASAD K., SUMAN C.K., CHOUDHARY R.N.P., Adv. Appl. Ceram., 105 (2006), 258.
[22] KRÖGER F.A., VINK H.J., Solid State Phys., 3 (1956), 307.
[23] PRASAD K., SUMAN C.K., CHOUDHARY R.N.P., Ferroelectrics, 324 (2005), 89.

Received 8 March 2009
Revised 4 June 2009